

www.acsami.org Research Article

Ion-Conducting Thermoresponsive Films Based on Polymer-Grafted Cellulose Nanocrystals

Ryo Kato, James H. Lettow, Shrayesh N. Patel,* and Stuart J. Rowan*



Cite This: ACS Appl. Mater. Interfaces 2020, 12, 54083–54093



ACCESS

Metrics & More

Article Recommendations

s Supporting Information

ABSTRACT: Mechanically robust, thermoresponsive, ion-conducting nanocomposite films are prepared from poly(2-phenylethyl methacrylate)-grafted cellulose nanocrystals (*MxG*-CNC-*g*-PPMA). One-component nanocomposite films of the polymergrafted nanoparticle (PGN) *MxG*-CNC-*g*-PPMA are imbibed with 30 wt % imidazolium-based ionic liquid to produce flexible ion-conducting films. These films with 1-hexyl-3-methylimidazolium bis(trifluoromethylsulfonyl)imide (*MxG*-CNC-*g*-PPMA/[H]) not only display remarkable improvements in toughness (>25 times) and tensile strength (>70 times) relative to the corresponding films consisting of the ionic liquid imbibed in the two-component CNC/PPMA nanocomposite but also show higher ionic conductivity than the corresponding neat PPMA with the same



weight percent of ionic liquid. Notably, the one-component film containing 1-ethyl-3-methylimidazolium bis-(trifluoromethylsulfonyl)imide (MxG-CNC-g-PPMA/[E]) exhibits temperature-responsive ionic conduction. The ionic conductivity decreases at around 60 °C as a consequence of the lower critical solution temperature phase transition of the grafted polymer in the ionic liquid, which leads to phase separation. Moreover, holding the MxG-CNC-g-PPMA/[E] film at room temperature for 24 h returns the film to its original homogenous state. These materials exhibit properties relevant to thermal cutoff safety devices (e.g., thermal fuse) where a reduction in conductivity above a critical temperature is needed.

KEYWORDS: thermal-responsive polymers, polymer-grafted nanoparticles, cellulose nanocrystals, smart materials, nanocomposites

■ INTRODUCTION

Smart materials that respond to external stimuli such as temperature, pH, solvent quality, pressure, light, etc. by changing their physical or chemical properties have been subject to extensive research.^{1,2} One class of temperature-sensitive polymers are those that exhibit a lower critical solution temperature (LCST).^{3–5} Such polymers are soluble in a solvent at low temperature but become insoluble as the temperature rises above the polymer's LCST. This class of responsive polymers has been commonly investigated in water and applied to a variety of smart thermoresponsive hydrogels with potential applications as actuators,^{6–8} separators,^{9,10} sensors,¹¹ etc. In addition, it has been shown that with aqueous-based LCST systems it is possible to inhibit ion transport/conduction as the temperature is raised above the LCST.^{12,13}

The temperature-induced phase transition of polymers has also been observed in ionic liquids. ^{14–16} Ionic liquids are molten salts with melting points lower than 100 °C¹⁷ and have been widely explored as solvents and/or electrolytes on account of their combination of physical properties that include nonvolatility, high thermal stability, wide electrochemical window, and high ionic conductivity. ^{18,19} As such,

composites of ionic liquids and polymers have also been studied and applied to various (quasi) solid materials, including new classes of electrolytes for batteries,²⁰ electrochemical actuators,²¹ transistors,²² gas separation membranes,²³ and 3D printing ionogels.^{24,25} Combining thermoresponsive polymers with an ionic liquid has the potential to expand the functionality of such solid materials and access a new generation of adaptive electrochemical polymeric systems. Furthermore, owing to a wide liquid temperature range, low volatility, and high thermal stability, ionic-liquid-containing materials can be used in an open atmosphere over extended periods without concerns about evaporation.

Poly(aryl methacrylates) are a class of polymers that are known to exhibit a LCST phase transition in certain imidazolium-based ionic liquids, which depending on the specific system can be tuned across a wide temperature range

Received: September 6, 2020 Accepted: November 9, 2020 Published: November 17, 2020





Scheme 1. Synthesis of MxG-CNC-g-poly(2-phenylethyl methacrylate) (MxG-CNC-g-PPMA) via the Grafting of H₂N-PPMA to Carboxylic-Acid-Functionalized CNCs (MxG-CNC-CO₂H) Using 4-(4,6-Dimethoxy-1,3,5-triazin-2-yl)-4-methylmorpholinium Tetrafluoroborate (DMTMMBF₄) as the Coupling Agent

(ca. 40–150 $^{\circ}$ C). One relevant example includes the work from Roberts and co-workers where they showed that dissolving poly(benzyl methacrylate) in an imidazoliumbased liquid electrolyte containing lithium salt resulted in the shutoff of a model lithium-ion battery at elevated temperatures.²⁷ The shutoff occurred on account of polymer aggregation and coating on the electrode surface when the temperature rose above the LCST transition of the polymer. Overall, while there are a number of reports of studies on LCST polymers in ionic liquids, most of these transitions are liquid—solid or sol—gel processes, ^{28–32} and there have been no reports, to the best of our knowledge, investigating the phase transition in more mechanically robust materials. Furthermore, in order to develop a separator or (quasi) solid electrolyte, it is important that the materials are mechanically robust enough to prevent short circuiting and/or thermal failure between electrodes.

A number of techniques have been employed to enhance the mechanical properties of LCST polymers. 33 The addition of nanofillers is a promising approach to allow access to composites with improved mechanical, thermal, and electrical properties.^{34,35} However, phase separation or demixing, especially at high filler loading, arising from poor fillerpolymer interactions remains an ongoing challenge. One strategy to address this issue is to graft the matrix polymer chains to the nanofiller (to yield polymer-grafted nanoparticles (PGNs)³⁶⁻³⁹) and to use those directly to access onecomponent nanocomposite (OCN) films. 40 Unlike conventional polymer nanocomposites that consist of at least two separate components (such as nanofiller and polymer matrix), the grafted polymer chains in OCNs suppress the aggregation of the nanofiller. OCNs remove the issue of component phase separation which results in more homogenous materials and improved melt processability. While most studies on OCNs have been carried out using spherical nanoparticles, the investigation of OCNs based on hairy nanorods is potentially appealing from the perspective of percolation. Cellulose nanocrystals (CNCs) are nanorods, which have been gathering significant attention as bio-based nanofillers that exhibit high

stiffness and strength. Al, 41,42 Recently, Weder and co-workers showed that CNCs grafted with poly(methyl or hexyl methacrylate) result in OCNs with superior mechanical properties to those of their two-component counterparts.

Reported herein are studies of OCN films of poly(2-phenylethyl methacrylate) (PPMA)-grafted CNCs with a specific focus on the thermomechanical and thermally-responsive ion conduction properties of such films imbibed with ionic liquid.

■ RESULTS AND DISCUSSION

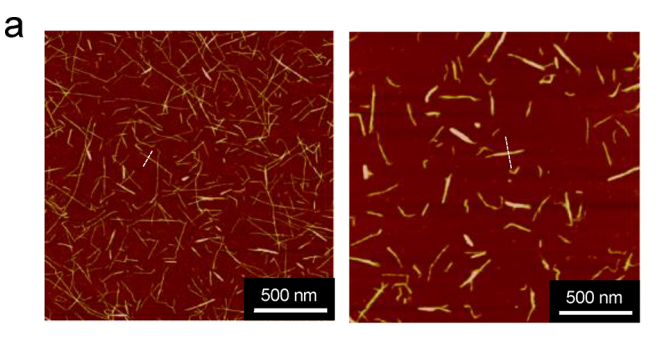
The synthetic route to access PPMA-grafted CNCs followed the attachment of amine-end-capped polymer chains onto carboxylic acid CNCs using standard peptide-coupling conditions (Scheme 1). Amine-end-capped PPMA (H₂N-PPMA) was synthesized via atom transfer radical polymerization (ATRP) of 2-phenylethyl methacrylate using N-(2-(2bromoisobutyryl)ethoxy)ethyl phthalimide as the initiator 44,45 followed by dehalogenation to yield the phthalimide-endcapped PPMA polymers (PhthN-PPMA). Deprotection of the phthalimidyl group then yields H2N-PPMA, which was prepared with different molecular weights, $M_n = 6100$, 9 800, and 20 000 g mol⁻¹, by controlling the reaction time and the initiator and monomer ratio (see the Supporting Information for more details). All three polymers had a dispersity (D) of ca. 1.3 as determined by GPC. Consistent with prior reports on PPMAs, ²⁶ the **PhthN-PPMA** (at 3 wt %) exhibited a LCST phase transition in 1-ethyl-3-methylimidazolium bis(trifluoromethylsulfonyl)imide ([EMIM][TFSI]) at ca. 41°C, while no such transition is observed in 1-hexyl-3methylimidazolium bis(trifluoromethylsulfonyl)imide ([HMIM][TFSI]) below 120 °C (Figure S1).

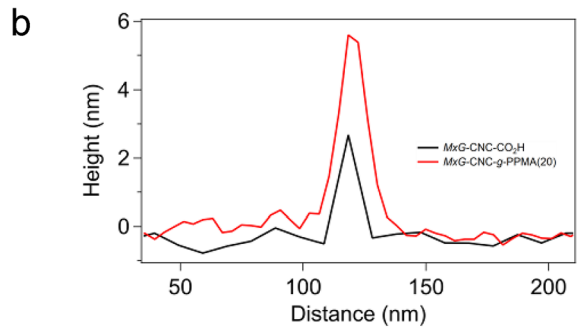
CNCs used in this study were isolated from *Miscanthus x. Giganteus* and oxidized via TEMPO-mediated oxidation to yield carboxylic-acid-functionalized CNCs (*MxG*-CNC-CO₂H). He *MxG*-CNC-CO₂Hs (carboxylic acid content: 870 mmol kg⁻¹) were functionalized with the amine-end-capped PPMAs (H₂N-PPMA) using 4-(4,6-dimethoxy-1,3,5-triazin-2-yl)-4-methylmorpholinium tetrafluoroborate

(DMTMMBF₄) as the coupling agent to yield the PPMAgrafted CNCs (MxG-CNC-g-PPMA(6), MxG-CNC-g-PPMA-(10), MxG-CNC-g-PPMA(20), where the number in parentheses represents the approximate molecular weight of the grafted PPMA in kg/mol). The MxG-CNC-g-PPMAs were thoroughly washed with acetone and THF via a centrifugation/ resuspension process at least eight times to remove any free polymer and other contaminants. The amount of free polymer removed after each wash was calculated by measuring the UV of the supernatant solution and comparing it to a calibration curve of the polymer concentration versus absorption intensity at 258 nm (Figure S3). By the fourth washing step most of the free polymer was removed (Table S1). A Kaiser test on the PPMA-grafted CNCs was carried out (in an ethanol/DMF (vol. 1/1) cosolvent) to test for the presence of amines: a purple color is observed for both the H2N-PPMA and unpurified product (Figure S2). After purification, all the MxG-CNC-g-PPMA samples did not elicit a color change, consistent with the removal of the unreacted PPMA via the washing protocol (Figure S2). Furthermore, UV studies show no evidence of a peak at ca. 580 nm that would correspond to a reacted amine moiety, confirming that the PGNs contain <2 wt % free polymer. AFM images (Figure 1a and b) show that there is an increase in the width and height of CNCs after the grafting reaction (e.g., the heights of MxG-CNC-CO2H and MxG-CNC-g-PPMA(20) were ca. 3.1 and ca. 5.5 nm, respectively), which is again consistent with the covalent functionalization of the PPMA on the surface of the CNCs.

The glass transition temperatures (T_g) (obtained from DSC) of all the MxG-CNC-g-PPMAs were higher than those of the corresponding PhthN-PPMA (Figure S4 and Table S2); for example, the T_g values of PhthN-PPMA(20) and MxG-CNC-g-PPMA(20) were 39 and 44 °C, respectively. This increase in T_g has been previously reported in other CNC-g-polymers 43,48 and can be attributed, in part, to the restricted chain mobility of the grafted polymer. Thermogravimetric analysis (TGA) shows no weight loss from the MxG-CNC-g-PPMA samples up to 200 °C (Figure 1c), and the weight ratio of grafted polymer to CNC could be calculated from the relative ratios of the remaining weight percent of H2N-PPMA(20), MxG-CNC-CO₂H, and MxG-CNC-g-PPMAs at 600 °C (see Table 1). As may be expected, the grafting density decreased with the increase of the molecular weight of PPMA presumably on account of the steric hindrance of the larger polymers; however, in all cases the weight ratio of PPMA:CNC in the MxG-CNC-g-PPMAs was >65 wt % (Table 1). Comparing the density of the polymer grafts with the simulation data of poly(methyl methacrylate)-grafted CNCs by Keten, 49 it can be estimated that MxG-CNC-g-PPMA(6) and MxG-CNC-g-PPMA(10) are in the concentrated polymer brush (CPB) regime, while MxG-CNC-g-PPMA(20) is in the concentrated polymer brush/semidilute polymer brush (CPB/ SDPB) regime.

All MxG-CNC-g-PPMAs could be processed into mechanically robust one-component transparent films by solvent casting. The resulting films did not show birefringence consistent with a lack of orientation of CNCs. Furthermore, a representative SEM of the solution cast MxG-CNC-g-PPMA(20) film (Figure SS) also shows no long-range order of the PGNs. The MxG-CNC-g-PPMA films were then swollen with a specific amount of [HMIM][TFSI]/THF or [EMIM]-[TFSI]/THF (vol. 1/1) solution. Subsequently, the samples were dried under vacuum (heated at 40 °C) to obtain an





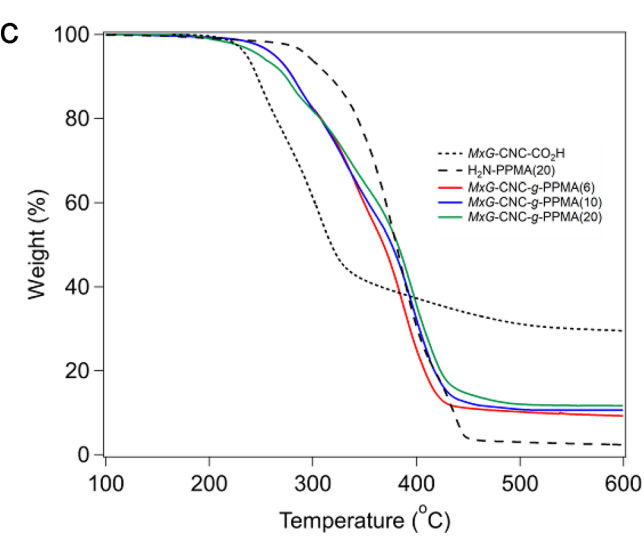


Figure 1. Characterization of the *MxG*-CNC-*g*-PPMAs. (a) AFM height image of *MxG*-CNC-CO₂H (left) and *MxG*-CNC-*g*-PPMA(20) (right). (b) AFM height profiles of *MxG*-CNC-CO₂H and *MxG*-CNC-*g*-PPMA(20). (c) Thermogravimetric analysis trace of *MxG*-CNC-CO₂H, H₂N-PPMA(20), *MxG*-CNC-*g*-PPMA(10), and *MxG*-CNC-*g*-PPMA(20).

electrolyte film (referred to as *MxG*-CNC-*g*-PPMA(6, 10, or 20)/[H] or [E]). After these swollen *MxG*-CNC-*g*-PPMA films were dried, it was shown that they were able to uptake ca. 35 wt % [HMIM][TFSI] or [EMIM][TFSI] with an excess of the ionic liquid/THF (vol. 1/1) solutions. Given that the CNCs are not expected to undergo any swelling in these ionic liquids, it is possible to calculate an effective maximum degree of swelling of the grafted polymer chains (Table 1). The grafted polymers in *MxG*-CNC-*g*-PPMA(20) swell more than those in *MxG*-CNC-*g*-PPMA(6) consistent with its lower grafting density. For all the following studies, the ionic liquid concentration was fixed at 30 wt % (relative to the total weight of film, seeTable S3 for a summary of the composition of these films). The amount of ionic liquid in the film after this swelling/drying protocol was verified by gravimetric analysis

Table 1. Weight Percent of Polymer and CNCs and Graft Density of the PGNs MxG-CNC-g-PPMAs and the Effective Maximum Degree of Swelling of the Polymer-Grafted Polymer Chains with [HMIM][TFSI]

sample	PPMA (wt %)	CNC (wt %)	grafting density (groups/nm²)	grafting density relative to the number of surface carboxyl groups $(\%)^a$	effective degree of maximum [HMIM][TFSI] swelling of the grafted polymer chains $(\%)^b$
MxG-CNC-g- PPMA(6)	72	28	0.43	50	74
MxG-CNC-g- PPMA(10)	67	33	0.21	24	80
MxG-CNC-g- PPMA(20)	65	35	0.10	11	83

^aThe ratio was calculated by $100 \times (grafting density)/(density of carboxylic acid groups = 0.87 groups/nm²). ^bThe effective degree of swelling of the grafted polymer chain is calculated by ((grafted PPMA weight after swelling with [HMIM][TFSI] – grafted PPMA weight before swelling)/grafted PPMA weight before swelling) × 100.$

(see the Supporting Information). For comparison, solution-cast two-component films (PhthN-PPMA(20)/CNC), which also did not show any birefringence, were imbibed with both of the ionic liquids (PhthN-PPMA(20)/CNC/[H] or [E]) at the same weight ratio of the components as the MxG-CNC-g-PPMA(20)/ionic liquid (i.e. 24 wt % MxG-CNC-CO₂H, 46 wt % PhthN-PPMA(20), and 30 wt % ionic liquid).

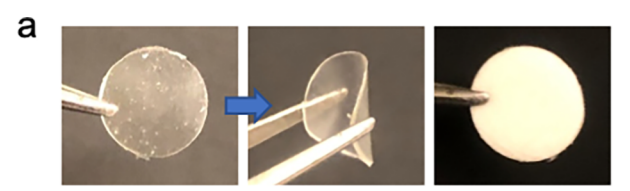
Figure 2a shows photographs of the resulting electrolyte-containing films. The opaque nature of the non-polymer-grafted composite film (PhthN-PPMA(20)/CNC/[H]) suggests that there is aggregation of the CNCs, an effect commonly observed in composites with >20 wt % of CNC. On the other hand, the polymer-grafted nanoparticle (PGN) electrolyte film (MxG-CNC-g-PPMA(20)/[H]) is optically clear, which is consistent with a more homogeneously dispersed film. Note that the ionic liquid does have a plasticizing effect on the PPMA (see Figure S6 and Table S2), where a significant decrease and broadening of the T_g is observed. For example, the T_g 's of MxG-CNC-g-PPMA(20)/[H] or [E] were around -10 °C, which is ca. 55 °C lower than those of the neat MxG-CNC-g-PPMA(20) films, and as a result, the one-component electrolyte films were flexible at room temperature.

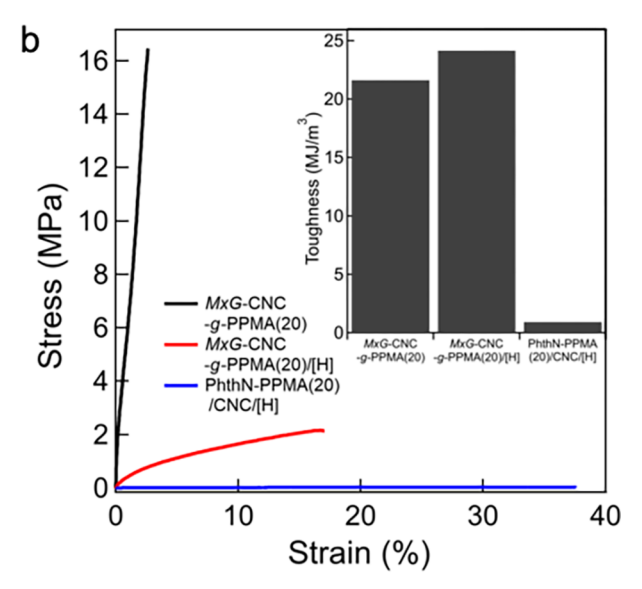
Tensile testing was performed at room temperature to characterize the mechanical properties of the PGN films with and without the [HMIM][TFSI] and the non-polymer-grafted film with [HMIM][TFSI] (Figure 2b). The one-component (or PGN) film (MxG-CNC-g-PPMA(20)) showed a relatively high tensile strength (16.5 MPa); however, the strain-at-break of the film was low (2.6%) owing to the film's above room temperature glass transition temperature ($T_{\rm g}$ ca. 45 °C). Note that the corresponding two-component PhthN-PPMA(20)/ CNC film was too brittle to test, which highlights the relative improvement in the mechanical properties of the OCN. As expected, the plasticization effect of the ionic liquid on the grafted PPMA polymer chains improved the strain-at-break value (ca. 17% for MxG-CNC-g-PPMA(20)/[H], T_g ca. -10°C) of the MxG-CNC-g-PPMA/[H] films. The toughness and maximum tensile strength of the PGN film with 30 wt % [HMIM][TFSI] were ca. 24 MJ m⁻³ and ca. 2 MPa, respectively. Furthermore, while the addition of 30 wt % [HMIM][TFSI] to the two-component film (PhthN-PPMA-(20)/CNC/[H]) resulted in a material that was able to undergo tensile testing, it exhibited a 27- and 72-times smaller toughness and maximum tensile strength, respectively, than the PGN MxG-CNC-g-PPMA(20)/[H] film (Figure 2a). However, the strain-at-break value of the ionic-liquid-containing PGN film was about half of that of the PhthN-PPMA(20)/ CNC/[H] film. It has been shown that PGNs based on

spherical nanoparticles and polymer grafts in the CPB/SDPB regime exhibit enhanced toughness. Extensive entanglements between the grafted polymer chains of a PGN have been suggested to result in this enhanced toughening. If, as suggested above, the MxG-CNC-g-PPMA(20) is in the CPB/SDPB regime, then the entanglement between the grafted polymer chains is certainly expected and, at least in part, can explain the enhanced toughness of these films.

Shear rheology experiments were performed to further investigate the mechanical properties of the [HMIM][TFSI]containing films (Figure 2c). While the polymer PhthN-PPMA(20) with 30 wt % [HMIM][TFSI] (PhthN-PPMA-(20)/[H]) exhibited a liquidlike behavior (shear storage modulus (G') < loss modulus (G'')) above 10 °C, both the ionic-liquid-containing composite films exhibited a solidlike behavior (G' > G''). It is interesting to note that the PGN film displayed a higher G' than its non-polymer-grafted counterpart; for example, the G' of the PGN film MxG-CNC-g-PPMA(20)/[H] was 3.5 MPa at 80 °C, ca. three times larger than that of non-grafted composite (PhthN-PPMA(20)/ CNC/[H]) film. In addition, the G' values of the PGN electrolyte films increase with the molecular weight of the grafted PPMA (Figure S7), presumably a consequence, at least in part, of the higher volume fraction of CNCs in the higher molecular weight samples (Table S3). It is worthy of note that all the PGN films exhibit a plateau modulus. A similar effect has been seen before⁴³ in related polymer-grafted CNCs and is presumably related to the PGN architecture and the grafted polymers being in the CPB/SDPB regime, which allows a significant number of chain entanglements between the grafted polymers of adjacent PGNs. It would be expected that at higher temperatures, the materials will start to flow, 43 but the rheology studies here were limited to lower temperatures as CNC composites are known to start to discolor and thermally degrade if held at higher temperatures (ca. 150 °C) for any length of time.

The ionic conductivity of the films containing [HMIM]-[TFSI], in which the PPMA does not exhibit a LCST transition below 120 °C, was investigated using AC electrochemical impedance spectroscopy in order to probe the effect of grafting the polymer to CNC (a representative Nyquist plot of a PGN film is shown in Figure S8). The ionic conductivity (σ) was subsequently calculated according to the equation $\sigma = L/(RA)$, where L is the thickness of the sample, A is the area of the sample, and R is the film resistance (experimentally obtained from impedance measurements). The ionic conductivities of both the polymer, PhthN-PPMA(20), and its two-component composite film imbibed with 30 wt % [HMIM][TFSI] were both around $3.4 \pm 1.8 \times 10^{-6}$ S cm⁻¹





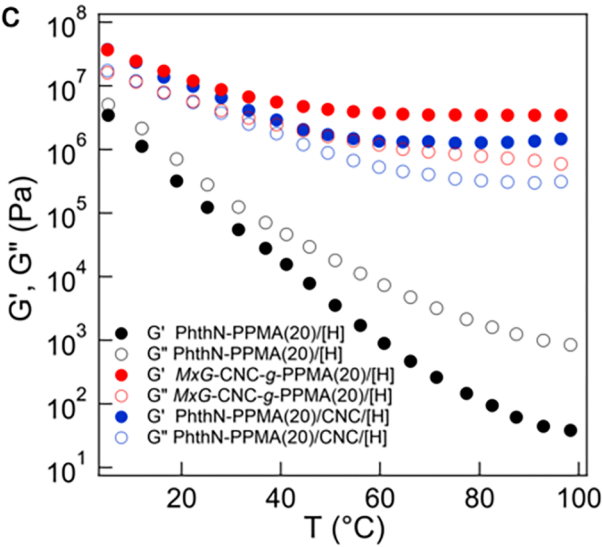


Figure 2. (a) Photographs of films of *MxG*-CNC-*g*-PPMA(20)/[H] (right) and PhthN-PPMA(20)/CNC/[H] (left). (b) Stress—strain curves and toughness values (inset) of the composite films with or without 30 wt % [HMIM][TFSI] (H) and (c) storage and loss modulus of PhthN-PPMA(20)/[H] and composite films with 30 wt % [HMIM][TFSI].

at 30 °C (Figure 3a). Interestingly, the one-component film imbibed with 30 wt % [HMIM][TFSI] film exhibited a slightly higher conductivity (5.7 \pm 2.1 \times 10⁻⁶ S cm⁻¹ at 30 °C). Furthermore, there is an increase in the conductivity of the ionic-liquid-containing PGNs as the molecular weight of the polymers grafts decreases, with *MxG*-CNC-*g*-PPMA(6)/[H] being ca. 2.9 \times 10⁻⁵ S cm⁻¹ at 30 °C and ca. 10⁻⁴ S cm⁻¹ at 50 °C. A summary of the films' ionic conductivities, at selected temperatures, can be found in Table S4. While these conductivities are not at the level for some applications, they

are within the range that has been used for sensors, electroactive actuators, and high-temperature energy storage devices.51-54 The activation energy of ion conduction was calculated using the Arrhenius equation, $\sigma(T) = A \exp(-E_2/E_1)$ RT), where $\sigma(T)$ is the ionic conductivity at temperature T, A is the pre-exponential factor, E_a is the activation energy, and Ris the ideal gas constant. The Ea of the PGN MxG-CNC-g-PPMA(20)/[H] was 53.2 kJ mol⁻¹, similar to both PhthN-PPMA(20)/[H] (53.9 kJ mol⁻¹) and PhthN-PPMA(20)/ CNC/[H] (54.3 kJ mol⁻¹) (Figure S9), and suggests a thermally activated ion conductivity mechanism in these materials. Furthermore, the ionic conductivity of the PGN electrolyte-containing film corrected for the weight percent of CNCs was larger than that of the non-polymer-grafted composite and the polymer with [HMIM][TFSI]. For example, the corrected ionic conductivity of MxG-CNC-g-**PPMA(20)/[H]** was 1.8×10^{-5} S cm⁻¹ at 30 °C which is ca. 3 and 1.5 times larger than those of the PhthN-PPMA/[H] and PhthN-PPMA(20)/CNC/[H] films, respectively (Figure S10). This higher conductivity might be explained through the interaction between the [HMIM][TFSI] and the hydroxyl groups on the surface of the CNCs (the density of surface hydroxyl groups on the polymer-grafted CNCs is ca. 9.8 groups/nm²), which improves ion dissociation and is in line with literature reports that have shown an enhancement of ionic conductivity in polymer nanocomposites with imidazolium-based ionic liquids or lithium salts. 55,56 The smaller increase in conductivity of the non-polymer-grafted CNC composite film may be on account of CNC aggregation which reduces the surface contact area.

It is worthy of note that even though the PGN films contain 28-35 wt % CNC, all of the PGN electrolyte-containing films (MxG-CNC-g-PPMA/[H]) irrespective of the molecular weight of the graft polymer consistently show higher ionic conductivity than the corresponding polymer with ionic liquid, PhthN-PPMA/[H] (Figure 3a and Table S4). While the weight ratio of the CNCs is slightly increased with the molecular weight of grafted PPMA, as mentioned before the ionic conductivity of the PGN films decreased with the increase of the molecular weight of grafted PPMA, a trend that was also observed with the polymer PhthN-PPMA/[H] (Figure S11). This behavior likely occurs on account of a decrease in viscosity.⁵⁷ Furthermore, the E_a's of the PGN films and the PhthN-PPMA/[H] decrease with the molecular weight of the polymers, which favors improved ion conduction (Figure S12 and Table S4).

Next, the ionic conductivity of the PGN film containing [EMIM][TFSI] (in which PPMA exhibits an LCST transition around 41 °C) was investigated. Figure 3b shows the ionic conductivity of the MxG-CNC-g-PPMA(20)/[E] film upon heating. The conductivity of the one-component film imbibed with [EMIM][TFSI] was nearly identical to that of the film imbibed with [HMIM][TFSI] below 50 °C. However, while the conductivity of the [HMIM][TFSI]-containing film increased with rising temperature (reaching 7.1×10^{-4} S cm⁻¹ at 120 °C) the ionic conductivity of the [EMIM][TFSI]imbibed film decreased around 60 $^{\circ}\text{C}$ and remained constant upon further increase in temperature $(5.4 \times 10^{-6} \text{ S cm}^{-1} \text{ at})$ 120 °C). This thermally-induced conductivity response of MxG-CNC-g-PPMA(20)/[E] is consistent with the collapse of grafted PPMA chains and phase separation at high temperature on account of the LCST phase transition, which in turn leads to a decrease of the ion mobility.

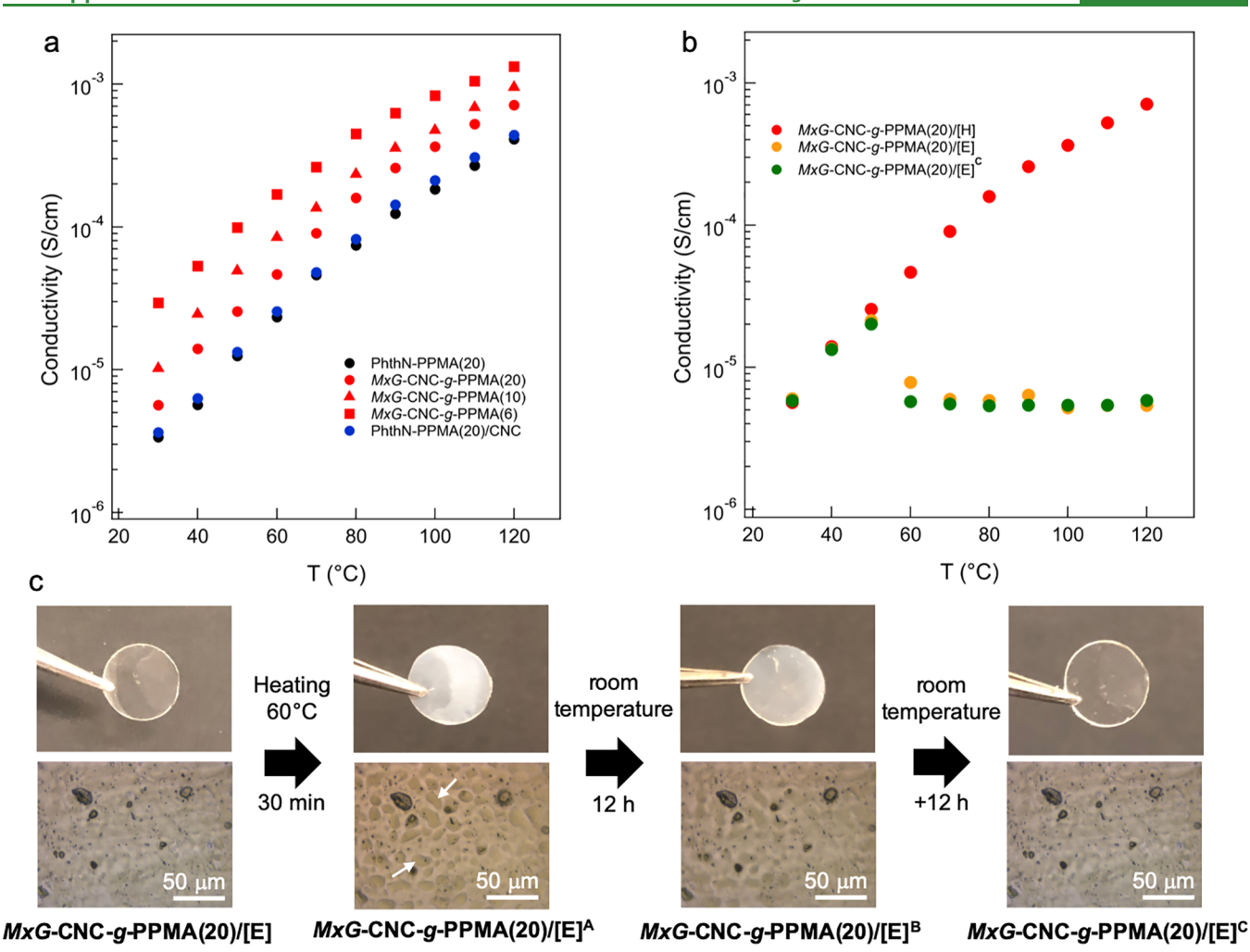


Figure 3. Temperature-dependent conductivity and thermal-responsive behavior of ionic-liquid-containing films. Temperature-dependent ionic conductivity of films (a) containing 30 wt % [HMIM][TFSI] and (b) containing 30 wt % [EMIM][TFSI] during a heating scan. (c) Photograph and microscope images of the PGN film containing 30 wt % [EMIM][TFSI].

Figure 3c shows images of the PGN film MxG-CNC-g-PPMA(20)/[E] before heating, the film after heating at 60 °C for 30 min (MxG-CNC-g-PPMA(20)/[E]A), and the film left at room temperature for 12 h (MxG-CNC-g-PPMA(20)/ $[E]^B$) and 24 h (MxG-CNC-g-PPMA $(20)/[E]^C$) after heating. The original MxG-CNC-g-PPMA(20)/[E] film was transparent; however, the MxG-CNC-g-PPMA(20)/ $[E]^A$ shows the expulsion of the ionic liquid and is opaque (Video S1 in the Supporting Information). In contrast, the appearance of the PGN film MxG-CNC-g-PPMA(20)/[H], which lacks a LCST, did not change after heating (Figure S13). At room temperature (i.e., below the LCST), the PPMA chains grafted on the CNCs are swollen with the ionic liquid, resulting in a transparent film. However, upon heating above the LCST, the polymer chains collapse, resulting in the extrusion of the ionic liquid and phase separation. Interestingly, after the film is held at room temperature for 24 h, the PGN film MxG-CNC-g-PPMA(20)/[E]^C is transparent once again with no obvious visible signs of phase separation, similar to the original onecomponent film. Additionally, the MxG-CNC-g-PPMA(20)/ [E]^C film exhibited the same ionic conductivity as the original film (Figure 2b). This slow reversible process presumably occurs from the slow diffusion of [EMIM][TFSI] back into the MxG-CNC-g-PPMA(20) phase, which is presumably a

consequence of the $T_{\rm g}$ of unswollen PPMA being above room temperature.

The DSC study also supports this slow reversible phase transition (Figure S14). The original PGN film with 30 wt % [EMIM][TFSI] (MxG-CNC-g-PPMA(20)/[E]) did not exhibit any crystallization/melting peaks that would correspond to pure [EMIM][TFSI] ionic liquid ($T_c = -50$ °C on cooling and $T_{\rm m} = -17$ °C on heating⁵⁸). This can be explained by the polymer chains interacting with the ionic liquid and inhibiting crystallization. However, sharp exothermic and endothermic peaks were observed at ca. -43 °C (cooling) and ca. -18 °C (heating) in the film that had just been heated above the LCST (MxG-CNC-g-PPMA(20)/[E]^A), and the T_{σ} of the film shifted from ca. -13 to ca. 30 °C, both of which are consistent with the phase separation of the polymer chains and ionic liquid. DSCs of MxG-CNC-g-PPMA(20)/[E]B and MxG-CNC-g-PPMA(20)/[E]^C show that over time at room temperature the exothermic and endothermic peaks slowly disappear and the $T_{\rm g}$ moves back to ca. 13 °C as the ionic liquid swells and plasticizes the PMMA chains.

The effect of this thermoresponse on the mechanical properties of the PGN electrolyte film was investigated (Figure S15). The shear rheology experiments of MxG-CNC-g-PPMA(20)/[E] showed a significant increase of G' (from ca. 5 to ca. 20 MPa at 1 Hz frequency) after heating the film at

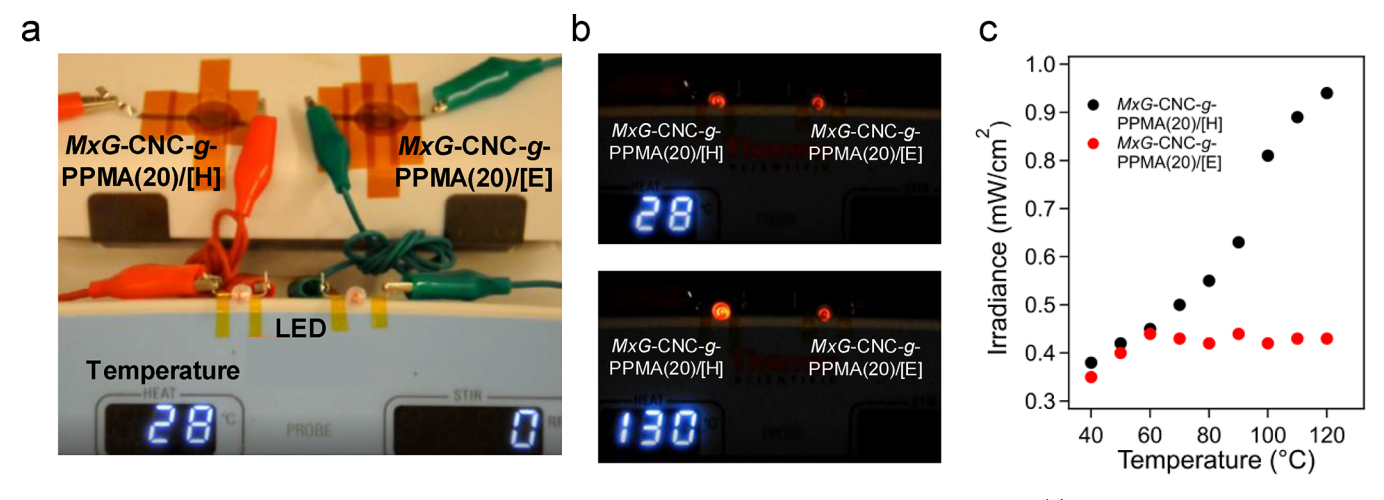


Figure 4. Visual demonstration of the thermal-responsive nature of the PGN—ionic liquid films. Photograph of (a) the experimental setup of *MxG*-CNC-*g*-PPMA(20)/[H] and *MxG*-CNC-*g*-PPMA(20)/[E] samples connected to a red LED and (b) the corresponding illuminated LED light at 28 and 130 °C. (c) Temperature dependence of LED irradiance.

60 °C (MxG-CNC-g-PPMA(20)/[E]^A in Figure S15b), while the G' of MxG-CNC-g-PPMA(20)/[H] (where PPMA does not exhibit an LCST transition) was relatively unchanged after heating. These data are again consistent with the LCST phase transition where the PPMA chains collapse and there is expulsion of the ionic liquid from the film. After 24 h at room temperature, the G' decreased to ca. 7 MPa at 1 Hz frequency, a value almost equivalent to that of the original film (MxG-CNC-g-PPMA(20)/[E]^C in Figure S15b).

Finally, to visualize the thermal-responsive nature of the PGN-ionic liquid films, MxG-CNC-g-PPMA(20)/[H] or [E] was placed between nickel foil electrodes, and power was applied across the electrodes using AA batteries in order to illuminate a red-light-emitting diode (LED). As shown in Figure 4 and Video S2 in the Supporting Information, the irradiance of the LED connected with the film containing [HMIM][TFSI] increased with temperature as would be expected. However, when using the film containing [EMIM]-[TFSI], the increase in irradiance was inhibited at temperatures above the LCST. These trends in the irradiance track well with the observed conductivity profile shown in Figure 3b, further emphasizing the coupling of thermally-induced phase transition and ion transport. The behavior of this film is potentially relevant to a thermal fuse, a class of thermal cutoff safety devices. Thermal fuses are incorporated within electronic circuitry in order to safely shut off operation by breaking electrical conduction upon going above a critical temperature. It is worth noting that a thermal fuse is typically a single use device. By leveraging the slow return of the conductivity at room temperature (Figure 3) of MxG-CNC-g-PPMA/[E], regenerable functionality can be potentially enabled for reusable thermal fuses.

CONCLUSIONS

In summary, ionic-liquid-containing films of the PGN *MxG*-CNC-*g*-PPMA have been shown to have improved both mechanical and conductive properties relative to their ionic-liquid-imbibed non-polymer-grafted composite counterparts. For example, the PGN film with [HMIM][TFSI] ionic liquid (*MxG*-CNC-*g*-PPMA(20)/[H]) displayed significant improvements in toughness (>25 times) and tensile strength (>70 times) in comparison to the corresponding non-polymer-

grafted nanocomposites. Additionally, MxG-CNC-g-PPMA-(20)/[H] exhibited higher ionic conductivity in comparison to the PPMA homopolymer and the non-polymer-grafted nanocomposite with [HMIM][TFSI] ionic liquid. Notably, the PGN film containing [EMIM][TFSI] (MxG-CNC-g-PPMA-(20)/[E]) exhibited a thermal response that resulted in a decrease in the ionic conductivity and an increase in the storage modulus by ca. 60 °C. These changes are consistent with the LCST phase transition of the PPMA chains, which leads to macrophase separation with the expulsion of the ionic liquid. Additionally, holding the MxG-CNC-g-PPMA/[E] film at room temperature for 24 h returned the film to its original state through the slow diffusion of [EMIM][TFSI] back into the polymer phase. The thermally-responsive conductive properties of MxG-CNC-g-PPMA/[E] have potential value for thermal cutoff safety devices (e.g., thermal fuse). A thermal fuse is a class of thermal cutoff devices where the electrical current is interrupted when heated above a critical temperature in order to prevent overheating. Thermal fuses are typically used in high-temperature appliances (e.g., coffee makers, power supplies, etc.). Here, these ion-conducting PGNs serve as an alternative material for a thermal fuse as the reduction in ionic conductivity above the LCST leads to the interruption of the electrical current. Overall, this work highlights the utility of polymer-grafted CNCs blended with an ionic liquid as mechanically robust PGN membranes with thermally responsive conductive properties that are broadly relevant to electronic and energy applications.

MATERIALS AND METHODS

Materials. 2-Phenylethyl methacrylate was purchased from Polysciences, Inc. *Miscanthus x. Giganteus* was generously donated by Aloterra Energy LLC, Conneaut, OH. 2-(2-Aminoethoxy)ethanol, phthalic anhydride, 2-bromoisobutyryl bromide, CuBr, CuBr₂, tin 2-ethylhexanoate, *N,N,N',N",N"*-pentamethyldiethylenetriamine (PMDETA), tributyltin hydride, hydrazine hydrate, 4-(4,6-dimethoxy-1,3,5-triazin-2-yl)-4-methylmorpholinium tetrafluoroborateand (DMTMMBF₄), polystyrene, polylysine, Kaiser test kit, and 1-hexyl-3-methylimidazolium bis(trifluormethylsulfonyl)imide were purchased from Sigma-Aldrich. All other reagents and solvents were purchased from Fisher Scientific.

Measurements. ¹H NMR spectra were recorded on a Bruker Ultrashield Plus 11.7T (500 MHz) spectrometer using tetramethylsilane as the internal standard. Molecular weight and dispersity of the

polymers were estimated by gel permeation chromatography using a Tosoh EcoSEC instrument and polystyrene standard calibration with N,N-dimethylformamide and Tosoh SuperAW3000 as the eluent and column, respectively. Differential scanning calorimetry (DSC) was carried out using a differential scanning calorimeter 2500 (TA Instruments Discovery), with a heating/cooling rate of 10 °C/min. Scanning electron microscope (SEM) images of the solution-cast films (from DMF) were taken with the Carl Zeiss-Merlin field emission scanning electron microscope. The acceleration voltage was 1.0 kV with a working distance of 2-3 mm using an in-lens detector. Two nanometers of Pt/Pd was sputtered onto the surface of the device using the Cressington 108 Auto Sputter Coater to reduce the electron beam charging and improve the image quality. Thermal gravimetric analysis (TGA) was carried out using a thermogravimetric analyzer (TA Instrument Discovery), and samples were heated from 30 to 600 °C under a nitrogen atmosphere at a heating rate of 10 °C/ min. Tensile testing was measured on a Zwick Roell Z0.5 Tensile tester (Zwick Roell, Germany) with a 500 N load cell at room temperature. Strips were stretched at a strain rate of 1 mm/min. The rheological properties were analyzed with an ARES-G2 rheometer (TA Instrument, USA) using a parallel-plate (8 mm diameter). Atomic force microscopy (AFM) was measured using a Bruker Multimode 8 instrument equipped with a Nanoscope 5 controller. Ionic conductivity was measured on a Biologic SP-200 potentiostat via frequency sweeps using a sinusoidal potential of 100 mV from 1 MHz to 100 mHz.

Synthesis of *N*-(2-(2-Bromoisobutyryl)ethoxy)ethyl Phthalimide. *N*-(2-(2-Bromoisobutyryl)ethoxy)ethyl phthalimide was synthesized according to previously published literature. 44,45 2-(2-Aminoethoxy)ethanol (5.3 g, 0.05 mol), phthalic anhydride (7.4 g, 0.05 mol), and THF (30 mL) were mixed and refluxed together for 2 h. THF was removed in vacuo, and the product was refluxed overnight in toluene (30 mL) using a Dean-Stark trap. The solution was cooled to 0 °C, triethylamine (5.1 g, 0.05 mol) and 2-bromoisobutyryl bromide (12.5 g, 0.05 mol) were added, and the solution was allowed to warm to room temperature and stirred for 3 h. After filtration, the solution was washed with NaCl aqueous solution (3 × 20 mL) and then filtered through a short plug of basic Al₂O₃. Removal of solvent in vacuo gave the yellow oil product. Yield: 15.6 g (81%); 1 H NMR (500 MHz, chloroform- 4 3, 5 3): 1.85 (s, 6H), 3.72 (t, 2H), 3.76 (t, 2H), 3.90 (t, 2H), 4.27 (t, 2H), 7.70-7.86 (m, 4H).

Synthesis of Phthalimide-end-capped Poly(2-phenylethyl methacrylate) (PhthN-PPMA). 2-Phenylethyl methacrylate (20.2 mL, 103.5 mmol), CuBr₂ (18.5 mg, 0.08 mmol), PMDETA (175 μ L, 0.82 mmol), and anisole (14 mL) were placed in a round-bottom flask and bubbled with nitrogen for 1 h. A purged solution of tin 2ethylhexanoate (268 µL, 0.82 mmol) and N-(2-(2-bromoisobutyryl)ethoxy)ethyl phthalimide (690 mg, 1.8 mmol) in anisole (6 mL) was added, and the sealed flask was placed in an oil bath at 40 °C. The polymerization was stopped after 20 or 60 min by opening the flask and diluting with THF. The polymerization mixture was passed through a basic Al₂O₃ column and poured into a large excess of cold methanol. The precipitate was dissolved in THF and reprecipitated in methanol three times and dried to yield poly(2-phenylethyl methacrylate) as a colorless powder. Yield = 9.1 g (41%), M_n = 6300, and D = 1.3, where the polymerization time was 20 min. When the polymerization was stopped after 60 min, the yield was 17.6 g (89%), $M_{\rm p}$ = 9900, and \bar{D} = 1.2.

The polymer with higher molecular weight was synthesized with a similar procedure as above. The polymerization condition was as follows: 2-phenylethyl methacrylate (40.4 mL, 209 mmol), CuBr₂ (9.2 mg, 0.04 mmol), PMDETA (87.6 μ L, 0.41 mmol), tin 2-ethylhexanoate (134 μ L, 0.41 mmol), N-(2-(2-bromoisobutyryl)ethoxy)ethyl phthalimide (345 mg, 0.9 mmol), and anisole (40 mL). The polymerization time was 3 h. Yield: 17 g (43%), M_n = 20 300, and D = 1.3; 1 H-NMR (500 MHz, dichloromethane- d_2 , δ): 7.18–7.32 (br, 5H), 4.19–4.12 (br, 2H), 2.93–2.83 (br, 2H), 2.85–2.69 (br, 2H), 0.82–0.62 (br, 3H)

All polymers were subsequently dehalogenated according to previously published literature. For example, polymer ($M_n = 20\,300$, 15 g), CuBr (50 mol %), PMEDTA (50 mol %), tributyltin hydride (300 mol %), and benzene 70 mL were placed in a round-bottom flask, bubbled with nitrogen for 30 min, and placed in an oil bath at 60 °C overnight. The reaction was stopped by opening the flask and diluting with THF. The mixture was passed through a basic Al₂O₃ column and poured into a large excess of cold methanol. The precipitate was dissolved in THF and reprecipitated in methanol two times and dried to yield dehalogenated **PhthN-PPMA** as a colorless powder. Yield: 12 g (80%), $M_n = 20\,200$, and D = 1.3; ¹H-NMR (500 MHz, dichloromethane- d_2 , δ): 7.19–7.32 (br, 5H), 4.19–4.13 (br, 2H), 2.91–2.83 (br, 2H), 2.85–2.70 (br, 2H), 0.82–0.63 (br, 3H)

Deprotection of PhthN-PPMA to Yield H₂N-PPMA. PhthN-PPMA was deprotected according to previously published literature. ^{44,45} For example, PhthN-PPMA ($M_{\rm n}=20\,200,\,10\,$ g, 0.5 mmol) was dissolved in 150 mL of THF in a round-bottom flask, followed by the addition of 1 mL of hydrazine hydrate. The reaction was refluxed for 2 h which resulted in the formation of a white precipitate (phthalhydrazide). The solution was centrifuged, and the top layer was precipitated in cold hexane. The precipitate was dissolved in THF and reprecipitated in cold hexane two times and dried to yield deprotected PhthN-PPMA as a colorless powder. Yield: 9 g (90%), $M_{\rm n}=20\,000,\,{\rm and}\,\, D=1.3;\,^{1}{\rm H-NMR}$ (500 MHz, dichloromethane- d_2 , δ): 7.18–7.32 (br, 5H), 4.19–4.13 (br, 2H), 2.91–2.83 (br, 2H), 2.84–2.69 (br, 2H), 0.82–0.63 (br, 3H).

Preparation of Carboxylic-Acid-Functionalized CNCs (*MxG*-CNC-CO₂H). CNCs were isolated from *Miscanthus Giganteus* (*MxG*) and oxidized by TEMPO-mediated oxidation according to the previously reported literature. ^{46,47} Following established procedures, ⁶⁰ the carboxylic acid content of the *MxG*-CNC-CO₂H was calculated by conductometric titration, and the charge density of *MxG*-CNC-CO₂H was 870 mmol/kg.

Synthesis of PPMA-Grafted CNCs (MxG-CNC-g-PPMA). MxG-CNC-g-PPMAs were synthesized by a grafting-to process using DMTMMBF₄ as the coupling agent. For example, a DMF suspension of MxG-CNC-CO₂H (18.5 g, 0.82 wt %) was prepared by a solventexchange method from water to acetone and then DMF and mixed with 4-(4,6-dimethoxy-1,3,5-triazin-2-yl)-4-methylmorpholinium tetrafluoroborate (DMTMMBF₄, 94 mg, 0.29 mmol), H₂N-PPMA(20) $(M_n = 20000, 4 g)$, and DMF (45 mL). The mixture was stirred overnight and precipitated in methanol followed by centrifugation. To ensure efficient removal of unreacted polymer, the resulting gel was dispersed in acetone, and a centrifugation/resuspension process was repeated four times. The same procedure was repeated using THF at least more four times to yield a transparent material after drying. The material before and after the washing process was dispersed in DMF (ca. 0.1 wt %) by ultrasonication and mixed with a Kaiser test kit solution purchased from Sigma-Aldrich containing KCN, Ninhydrin, phenol, ethanol, water, and pyridine.

The weight ratio of grafted polymer to CNC was calculated from TGA results according to the following equation:

weight ratio of grafted polymer (wt %)

$$= \frac{W_{\text{CNC}} - W_{\text{CNC-}g-PPMA}}{W_{\text{CNC}} - W_{\text{PPMA}}} \times 100$$

where $W_{\rm CNC}$ is the residue wt % of MxG-CNC-CO $_2$ H at 600 °C, $W_{\rm PPMA}$ is the residue wt % of H_2 N-PPMA(20) at 600 °C, and $W_{\rm CNC-g\text{-}PPMA}$ is the residue wt % of MxG-CNC-g-PPMA at 600 °C. Calculation of the Polymer-Grafting Density. In order to

Calculation of the Polymer-Grafting Density. In order to estimate the grafting density of the PPMA on the CNCs, it was assumed that the crystal structure of CNCs isolated from MxG is cellulose $I\beta$, and the calculation employed followed the previously reported literature. The cross section of CNCs isolated from MxG for simplification can be modeled as a rectangle with an average dimension of the long and short side of L=8.5 nm and l=2.8 nm. In the cellulose $I\beta$ crystal, the distance between each cellulose chain is 0.61 nm parallel to the long side of the rectangular cross section and 0.54 nm parallel to the short side. Thus, within this average crystal,

there are $8.5 \times 2.8/0.61 \times 0.54 = 72$ cellulose chains. In this crystal, the number of surface cellulose chains is therefore 2(8.5/0.54) + 2(2.8/0.61) = 41 cellulose chains, and the ratio of surface cellulose chains to the total number of cellulose chains in the crystal is 0.56. The average surface area of one anhydroglucose unit is 0.28 nm².⁶³

Hence, the grafting density of the polymer was calculated using the following equation

$${\rm grafting~density~(groups/nm}^2) = \frac{M_{\rm glucose}W_{\rm polymer}}{M_{\rm polymer}W_{\rm CNC}\times 0.56\times 0.28}$$

where $M_{
m glucose}$ is the molecular weight of anhydroglucose (162 g/mol), $M_{
m polymer}$ is the molecular weight of the polymer, $W_{
m CNC}$ is the weight ratio of CNC, and $W_{
m polymer}$ is the weight ratio of the polymer. Preparation of 1-Ethyl-3-methylimidazolium Bis-

Preparation of 1-Ethyl-3-methylimidazolium Bis-(trifluoromethylsulfonyl)imide ([EMIM][TFSI]). 1-Ethyl-3-methylimidazolium bis(trifluoromethylsulfonyl)imide ([EMIM][TFSI]) was prepared by ion-exchange according to the previously reported literature. 10 1-Ethyl-3-methylimidazolium bromide was dissolved in water, and an aqueous solution of lithium bis(trifluoromethane sulfonyl)imide (1.1 equiv) was added dropwise with vigorous stirring. The organic phase was separated and washed with water until the remaining bromide ions were undetected with an AgNO₃ solution. The solvent was evaporated, and the remaining viscous liquid was dried under vacuum at 60 °C for 3 days.

Preparation of the One-/Two-Component Electrolyte Film. One-component films were prepared by solvent casting. For example, MxG-CNC-g-PPMA was dispersed in DMF via ultrasonication (MxG-CNC-CO₂H: 0.45 wt %) and poured into a Teflon dish (diameter: 5 mm). The suspension was dried under vacuum with heating (60 °C) for 4 days to yield a robust transparent film. The desired amount of ionic liquid (30 wt %) was imbibed into the film by swelling the film with a specific volume of [HMIM][TFSI] or [EMIM][TFSI]/THF (vol. 1/1) solutions. Subsequently, the film was dried under vacuum (heated at 40 °C) to obtain a one-component electrolyte film (thickness: ca. 250 μ m). The weight of the dried onecomponent electrolyte film was measured, and the weight of ionic liquid loaded into the one-component film was estimated according to the following equation, $w = w_1 - w_0$, where w is the weight of the ionic liquid in the film, w_0 is the measured weight of the dried onecomponent film, and w_1 is the measured weight of the dried film after the ionic liquid imbibing process.

To access the two-component electrolyte film MxG-CNC-CO₂H (24 wt %), PhthN-PPMA(20) (46 wt %), and ionic liquid (30 wt %) were mixed in DMF via ultrasonication and poured into a Teflon dish. The suspension was dried under vacuum at 60 °C for 4 days (thickness: ca. 230 μ m).

Atomic Force Microscopy (AFM). The surface topographies of MxG-CNC-CO₂H and MxG-CNC-g-PPMA(20) were characterized by AFM with a silicon nitride probe (Bruker ScanAsyst-Air). MxG-CNC-CO₂H (0.01 wt %) was dispersed in water, and then a drop of the suspension was placed on a freshly cleaved mica surface that has been pretreated with polylysine. After 5 min, the excess dispersion was rinsed off with water, and the sample was dried in a fumehood overnight. The sample of MxG-CNC-g-PPMA(20) was also prepared using a similar procedure but was dispersed in DMF and dried under vacuum at 60 °C for 2 days. The images were acquired using the ScanAsyst mode. The height was analyzed by using Gwyddion software.

Ionic Conductivity Measurements. Disc-shaped one- or two-component electrolyte films were punched out using a hand punch of diameter 4 mm and dried under vacuum at 40 $^{\circ}$ C in a glovebox antechamber to remove residual moisture and then directly moved into the glovebox without air exposure. The dried film was placed in the center of a kapton washer (ca. 200 μ m thickness) with an outer diameter of 16 mm and inner hole diameter of 4 mm. Then, nickel foil current collectors were place on both sides. The sample was placed in the air-tight holder to perform conductivity measurements. All cell samples were gently pressed during the conductivity measurement to ensure good contact between the nickel electrode and polymer film.

Ionic conductivity values were determined using electrochemical impedance spectroscopy. The resistance (R) of the ionic-liquid-containing polymer samples was extracted from the real (Z') component of the complex impedance $(Z^* = Z' - i\omega Z'')$. The value of R was converted to ionic conductivity (σ) by accounting for the sample geometry, $\sigma = L/(RA)$, where L is the thickness and A is the area of the polymer film.

Demonstration Test. The effect of the thermal-responsive nature of one-component electrolyte films MxG-CNC-g-PPMA(20)/[H] or [E] was demonstrated as follows; the one-component electrolyte film was punched out using a hand punch of diameter 8 mm and placed in the center of a kapton washer (ca. 200 μ m thickness) with an outer diameter of 16 mm and inner hole diameter of 8 mm. Then, the nickel foil current collectors were placed on both sides. The sample was placed on the hot plate, and the cell was connected with AA batteries and a light-emitting diode (LED). The irradiance of LED was measured by an UV-meter (Honle UV technology).

ASSOCIATED CONTENT

Supporting Information

The Supporting Information is available free of charge at https://pubs.acs.org/doi/10.1021/acsami.0c16059.

Figures S1-S15 and and Tables S1-S4 as described in the main text (PDF)

Microscope images of the one-component film containing [EMIM][TFSI] (MP4)

Visual demonstration of the thermal responsive nature of the one-component electrolyte films (MP4)

AUTHOR INFORMATION

Corresponding Authors

Stuart J. Rowan — Pritzker School for Molecular Engineering and Department of Chemistry, University of Chicago, Chicago, Illinois 60637, United States; Joint Center for Energy Storage Research and Chemical Sciences and Engineering Division, Argonne National Laboratory, Lemont, Illinois 60439, United States; Occid.org/0000-0001-8176-0594; Email: stuartrowan@uchicago.edu

Shrayesh N. Patel — Pritzker School for Molecular Engineering, University of Chicago, Chicago, Illinois 60637, United States; Joint Center for Energy Storage Research and Chemical Sciences and Engineering Division, Argonne National Laboratory, Lemont, Illinois 60439, United States; orcid.org/0000-0003-3657-827X; Email: shrayesh@uchicago.edu

Authors

Ryo Kato – Pritzker School for Molecular Engineering, University of Chicago, Chicago, Illinois 60637, United States; Joint Center for Energy Storage Research, Argonne National Laboratory, Lemont, Illinois 60439, United States

James H. Lettow – Pritzker School for Molecular Engineering, University of Chicago, Chicago, Illinois 60637, United States

Complete contact information is available at: https://pubs.acs.org/10.1021/acsami.0c16059

Author Contributions

The manuscript was written through contributions of all authors. All authors have given approval to the final version of the manuscript.

Notes

The authors declare no competing financial interest.

ACKNOWLEDGMENTS

Funding for this project was provided by the U.S. Army Research Office (ARO) under grant numbers W911NF-15-1-0190 and W911NF-18-1-0287 (synthesis and mechanical testing) and partial support from the Joint Center for Energy Storage Research (JCESR), an Energy Innovation Hub funded by the U.S. Department of Energy, Office of Science, Basic Energy Sciences (BES) under Contract DE-AC02-06CH11357 (conductivity studies). Parts of this work were carried out at the Soft Matter Characterization Facility of the University of Chicago. This work made use of the shared facilities at the University of Chicago Materials Research Science and Engineering Center, supported by the National Science Foundation under award numbers DMR-1420709 and DMR-2011854.

REFERENCES

- (1) Pasparakis, G.; Vamvakaki, M. Multiresponsive Polymers: Nano-Sized Assemblies, Stimuli-Sensitive Gels and Smart Surfaces. *Polym. Chem.* **2011**, 2 (6), 1234–1248.
- (2) Jochum, F. D.; Theato, P. Temperature- and Light-Responsive Smart Polymer Materials. *Chem. Soc. Rev.* **2013**, 42 (17), 7468–7483.
- (3) Wei, H.; Cheng, S. X.; Zhang, X. Z.; Zhuo, R. X. Thermo-Sensitive Polymeric Micelles Based on Poly(N-Isopropylacrylamide) as Drug Carriers. *Prog. Polym. Sci.* **2009**, *34* (9), 893–910.
- (4) Adhikari, S.; Prabhu, V. M.; Muthukumar, M. Lower Critical Solution Temperature Behavior in Polyelectrolyte Complex Coacervates. *Macromolecules* **2019**, *52* (18), 6998–7004.
- (5) Strandman, S.; Zhu, X. X. Thermo-Responsive Block Copolymers with Multiple Phase Transition Temperatures in Aqueous Solutions. *Prog. Polym. Sci.* **2015**, *42*, 154–176.
- (6) Zheng, J.; Xiao, P.; Le, X.; Lu, W.; Théato, P.; Ma, C.; Du, B.; Zhang, J.; Huang, Y.; Chen, T. Mimosa Inspired Bilayer Hydrogel Actuator Functioning in Multi-Environments. *J. Mater. Chem. C* **2018**, 6 (6), 1320–1327.
- (7) Zheng, W. J.; An, N.; Yang, J. H.; Zhou, J.; Chen, Y. M. Tough Al-Alginate/Poly(N -Isopropylacrylamide) Hydrogel with Tunable LCST for Soft Robotics. ACS Appl. Mater. Interfaces 2015, 7 (3), 1758–1764
- (8) Jiang, S.; Liu, F.; Lerch, A.; Ionov, L.; Agarwal, S. Unusual and Superfast Temperature-Triggered Actuators. *Adv. Mater.* **2015**, *27* (33), 4865–4870.
- (9) Ito, T.; Hioki, T.; Yamaguchi, T.; Shinbo, T.; Nakao, S. I.; Kimura, S. Development of a Molecular Recognition Ion Gating Membrane and Estimation of Its Pore Size Control. *J. Am. Chem. Soc.* **2002**, *124* (26), 7840–7846.
- (10) Jiang, H.; Emmett, R. K.; Roberts, M. E. Building Thermally Stable Supercapacitors Using Temperature-Responsive Separators. *J. Appl. Electrochem.* **2019**, 49 (3), 271–280.
- (11) Koopmans, C.; Ritter, H. Color Change of N-Isopropylacry-lamide Copolymer Bearing Reichardts Dye as Optical Sensor for Lower Critical Solution Temperature and for Host-Guest Interaction with β -Cyclodextrin. J. Am. Chem. Soc. 2007, 129 (12), 3502–3503.
- (12) Yang, H.; Leow, W. R.; Chen, X. Thermal-Responsive Polymers for Enhancing Safety of Electrochemical Storage Devices. *Adv. Mater.* **2018**, *30* (13), 1704347.
- (13) Shi, Y.; Ha, H.; Al-Sudani, A.; Ellison, C. J.; Yu, G. Thermoplastic Elastomer-Enabled Smart Electrolyte for Thermoresponsive Self-Protection of Electrochemical Energy Storage Devices. *Adv. Mater.* **2016**, 28 (36), 7921–7928.
- (14) Lee, H. N.; Lodge, T. P. Lower Critical Solution Temperature (LCST) Phase Behavior of Poly(Ethylene Oxide) in Ionic Liquids. *J. Phys. Chem. Lett.* **2010**, *1* (13), 1962–1966.
- (15) Ueki, T.; Watanabe, M. Lower Critical Solution Temperature Behavior of Linear Polymers in Ionic Liquids and the Corresponding Volume Phase Transition of Polymer Gels. *Langmuir* **2007**, 23 (3), 988–990.

- (16) Lee, H. N.; Newell, N.; Bai, Z.; Lodge, T. P. Unusual Lower Critical Solution Temperature Phase Behavior of Poly(Ethylene Oxide) in Ionic Liquids. *Macromolecules* **2012**, *45* (8), 3627–3633.
- (17) Watanabe, M.; Thomas, M. L.; Zhang, S.; Ueno, K.; Yasuda, T.; Dokko, K. Application of Ionic Liquids to Energy Storage and Conversion Materials and Devices. *Chem. Rev.* **2017**, *117* (10), 7190–7239
- (18) Macfarlane, D. R.; Tachikawa, N.; Forsyth, M.; Pringle, J. M.; Howlett, P. C.; Elliott, G. D.; Davis, J. H.; Watanabe, M.; Simon, P.; Angell, C. A. Energy Applications of Ionic Liquids. *Energy Environ. Sci.* **2014**, 7 (1), 232–250.
- (19) Lozano, L. J.; Godínez, C.; de los Ríos, A. P.; Hernández-Fernández, F. J.; Sánchez-Segado, S.; Alguacil, F. J. Recent Advances in Supported Ionic Liquid Membrane Technology. *J. Membr. Sci.* **2011**, *376* (1-2), 1–14.
- (20) Ichikawa, T.; Kato, T.; Ohno, H. Dimension Control of Ionic Liquids. Chem. Commun. 2019, 55 (57), 8205-8214.
- (21) Zhou, D.; Spinks, G. M.; Wallace, G. G.; Tiyapiboonchaiya, C.; MacFarlane, D. R.; Forsyth, M.; Sun, J. Solid State Actuators Based on Polypyrrole and Polymer-in-Ionic Liquid Electrolytes. *Electrochim. Acta* **2003**, 48 (14-16), 2355–2359.
- (22) Xia, Y.; Cho, J. H.; Lee, J.; Ruden, P. P.; Frisbie, C. D. Comparison of the Mobility-Carrier Density Relation in Polymer and Single-Crystal Organic Transistors Employing Vacuum and Liquid Gate Dielectrics. *Adv. Mater.* **2009**, *21* (21), 2174–2179.
- (23) Kasahara, S.; Kamio, E.; Ishigami, T.; Matsuyama, H. Amino Acid Ionic Liquid-Based Facilitated Transport Membranes for CO 2 Separation. *Chem. Commun.* **2012**, *48* (55), 6903–6905.
- (24) Wong, J.; Gong, A. T.; Defnet, P. A.; Meabe, L.; Beauchamp, B.; Sweet, R. M.; Sardon, H.; Cobb, C. L.; Nelson, A. 3D Printing Ionogel Auxetic Frameworks for Stretchable Sensors. *Adv. Mater. Technol.* **2019**, *4* (9), 1900452.
- (25) Wong, J.; Basu, A.; Wende, M.; Boechler, N.; Nelson, A. Mechano-Activated Objects with Multidirectional Shape Morphing Programmed via 3D Printing. ACS Appl. Polym. Mater. 2020, 2, 2504.
- (26) Kodama, K.; Nanashima, H.; Ueki, T.; Kokubo, H.; Watanabe, M. Lower Critical Solution Temperature Phase Behavior of Linear Polymers in Imidazolium-Based Ionic Liquids: Effects of Structural Modifications. *Langmuir* **2009**, 25 (6), 3820–3824.
- (27) Kelly, J. C.; Degrood, N. L.; Roberts, M. E. Li-Ion Battery Shutoff at High Temperature Caused by Polymer Phase Separation in Responsive Electrolytes. *Chem. Commun.* **2015**, *51* (25), 5448–5451.
- (28) He, Y.; Lodge, T. P. A Thermoreversible Ion Gel by Triblock Copolymer Self-Assembly in an Ionic Liquid. *Chem. Commun.* **2007**, No. 26, 2732–2734.
- (29) Kitazawa, Y.; Ueki, T.; Niitsuma, K.; Imaizumi, S.; Lodge, T. P.; Watanabe, M. Thermoreversible High-Temperature Gelation of an Ionic Liquid with Poly(Benzyl Methacrylate-b-Methyl Methacrylate-b-Benzyl Methacrylate) Triblock Copolymer. *Soft Matter* **2012**, 8 (31), 8067–8074.
- (30) Lodge, T. P.; Ueki, T. Mechanically Tunable, Readily Processable Ion Gels by Self-Assembly of Block Copolymers in Ionic Liquids. *Acc. Chem. Res.* **2016**, 49 (10), 2107–2114.
- (31) Tamate, R.; Hashimoto, K.; Ueki, T.; Watanabe, M. Block Copolymer Self-Assembly in Ionic Liquids. *Phys. Chem. Chem. Phys.* **2018**, 20 (39), 25123–25139.
- (32) Ueki, T.; Nakamura, Y.; Usui, R.; Kitazawa, Y.; So, O.; Lodge, T. P.; Watanabe, M. Photoreversible Gelation of a Triblock Copolymer in an Ionic Liquid. *Angew. Chem., Int. Ed.* **2015**, 54 (10), 3018–3022.
- (33) Haq, M. A.; Su, Y.; Wang, D. Mechanical Properties of PNIPAM Based Hydrogels: A Review. *Mater. Sci. Eng., C* **2017**, 70, 842–855.
- (34) Mishra, A. K.; Bose, S.; Kuila, T.; Kim, N. H.; Lee, J. H. Silicate-Based Polymer-Nanocomposite Membranes for Polymer Electrolyte Membrane Fuel Cells. *Prog. Polym. Sci.* **2012**, *37* (6), 842–869.
- (35) Schexnailder, P.; Schmidt, G. Nanocomposite Polymer Hydrogels. *Colloid Polym. Sci.* **2009**, 287 (1), 1-11.

- (36) Chancellor, A. J.; Seymour, B.; Zhao, B. Characterizing Polymer-Grafted Nanoparticles: From Basic Defining Parameters to Behavior in Solvents and Self-Assembled Structures. *Anal. Chem.* **2019**, *91* (10), *6391–6402*.
- (37) Hore, M. J. A.; Korley, L. T. J.; Kumar, S. K. Polymer-Grafted Nanoparticles. *J. Appl. Phys.* **2020**, *128* (3), 030401.
- (38) Hore, M. J. A. Polymers on Nanoparticles: Structure & Dynamics. Soft Matter 2019, 15 (6), 1120–1134.
- (39) Kumar, S. K.; Jouault, N.; Benicewicz, B.; Neely, T. Nanocomposites with Polymer Grafted Nanoparticles. *Macromolecules* **2013**, *46* (9), 3199–3214.
- (40) Fernandes, N. J.; Koerner, H.; Giannelis, E. P.; Vaia, R. A. Hairy Nanoparticle Assemblies as One-Component Functional Polymer Nanocomposites: Opportunities and Challenges. *MRS Commun.* **2013**, 3 (1), 13–29.
- (41) Moon, R. J.; Martini, A.; Nairn, J.; Simonsen, J.; Youngblood, J. Cellulose Nanomaterials Review: Structure, Properties and Nanocomposites. *Chem. Soc. Rev.* **2011**, *40* (7), 3941.
- (42) Calvino, C.; Macke, N.; Kato, R.; Rowan, S. J. Development, Processing and Applications of Bio-Sourced Cellulose Nanocrystal Composites. *Prog. Polym. Sci.* **2020**, *103*, 101221.
- (43) Wohlhauser, S.; Kuhnt, T.; Meesorn, W.; Montero De Espinosa, L.; Zoppe, J. O.; Weder, C. One-Component Nanocomposites Based on Polymer-Grafted Cellulose Nanocrystals. *Macromolecules* **2020**, *53*, 821–834.
- (44) Harrisson, S.; Drisko, G. L.; Malmström, E.; Hult, A.; Wooley, K. L. Hybrid Rigid/Soft and Biologic/Synthetic Materials: Polymers Grafted onto Cellulose Microcrystals. *Biomacromolecules* **2011**, *12* (4), 1214–1223.
- (45) Cudjoe, E.; Khani, S.; Way, A.; Hore, M.; Maia, J.; Rowan, S. Biomimetic Reversible Heat-Stiffening Polymer Nanocomposites. *ACS Cent. Sci.* **2017**, *3* (8), 886–894.
- (46) Cudjoe, E.; Hunsen, M.; Xue, Z.; Way, A. E.; Barrios, E.; Olson, R. A.; Hore, M. J. A.; Rowan, S. J. Miscanthus Giganteus: A Commercially Viable Sustainable Source of Cellulose Nanocrystals. *Carbohydr. Polym.* **2017**, *155*, 230–241.
- (47) Yang, H.; Zhang, Y.; Kato, R.; Rowan, S. J. Preparation of Cellulose Nanofibers from Miscanthus x. Giganteus by Ammonium Persulfate Oxidation. *Carbohydr. Polym.* **2019**, 212, 30–39.
- (48) Zhang, Z.; Tam, K. C.; Sebe, G.; Wang, X. Convenient Characterization of Polymers Grafted on Cellulose Nanocrystals via SI-ATRP without Chain Cleavage. *Carbohydr. Polym.* **2018**, *199* (July), 603–609.
- (49) Hansoge, N. K.; Keten, S. Effect of Polymer Chemistry on Chain Conformations in Hairy Nanoparticle Assemblies. *ACS Macro Lett.* **2019**, 8 (10), 1209–1215.
- (50) Jiao, Y.; Tibbits, A.; Gillman, A.; Hsiao, M. S.; Buskohl, P.; Drummy, L. F.; Vaia, R. A. Deformation Behavior of Polystyrene-Grafted Nanoparticle Assemblies with Low Grafting Density. *Macromolecules* **2018**, *51* (18), 7257–7265.
- (51) Mostafavi, E.; Medina-Cruz, D.; Kalantari, K.; Taymoori, A.; Soltantabar, P.; Webster, T. J. Electroconductive Nanobiomaterials for Tissue Engineering and Regenerative Medicine. *Bioelectricity* **2020**, 2 (2), 120–149.
- (52) Yan, Y.; Santaniello, T.; Bettini, L. G.; Minnai, C.; Bellacicca, A.; Porotti, R.; Denti, I.; Faraone, G.; Merlini, M.; Lenardi, C.; et al. Electroactive Ionic Soft Actuators with Monolithically Integrated Gold Nanocomposite Electrodes. *Adv. Mater.* **2017**, 29 (23), 1606109.
- (53) Wei, P.; Chen, T.; Chen, G.; Liu, H.; Mugaanire, I. T.; Hou, K.; Zhu, M. Conductive Self-Healing Nanocomposite Hydrogel Skin Sensors with Antifreezing and Thermoresponsive Properties. *ACS Appl. Mater. Interfaces* **2020**, *12* (2), 3068–3079.
- (\$4) Lin, X.; Salari, M.; Arava, L. M. R.; Ajayan, P. M.; Grinstaff, M. W. High Temperature Electrical Energy Storage: Advances, Challenges, and Frontiers. *Chem. Soc. Rev.* **2016**, 45 (21), 5848–5887.
- (55) Liu, W.; Lin, D.; Sun, J.; Zhou, G.; Cui, Y. Improved Lithium Ionic Conductivity in Composite Polymer Electrolytes with Oxide-Ion Conducting Nanowires. *ACS Nano* **2016**, *10* (12), 11407–11413.

- (56) Kim, D.; Kannan, P. K.; Chung, C. H. High-Performance Flexible Supercapacitors Based on Ionogel Electrolyte with an Enhanced Ionic Conductivity. *Chemistry Select* **2018**, 3 (7), 2190–2195
- (57) Kumar, R.; Sekhon, S. S. Effect of Molecular Weight of PMMA on the Conductivity and Viscosity Behavior of Polymer Gel Electrolytes Containing NH4CF3SO3. *Ionics* **2008**, *14* (6), 509–514.
- (58) Fredlake, C. P.; Crosthwaite, J. M.; Hert, D. G.; Aki, S. N. V. K.; Brennecke, J. F. Thermophysical Properties of Imidazolium-Based Ionic Liquids. *J. Chem. Eng. Data* **2004**, 49 (4), 954–964.
- (59) Coessens, V.; Matyjaszewski, K. Dehalogenation of Polymers Prepared by Atom Transfer Radical Polymerization. *Macromol. Rapid Commun.* **1999**, 20 (2), 66–70.
- (60) Way, A. E.; Hsu, L.; Shanmuganathan, K.; Weder, C.; Rowan, S. J. PH-Responsive Cellulose Nanocrystal Gels and Nanocomposites. *ACS Macro Lett.* **2012**, *1*, 1001.
- (61) Okita, Y.; Saito, T.; Isogai, A. Entire Surface Oxidation of Various Cellulose Microfibrils by TEMPO-Mediated Oxidation. *Biomacromolecules* **2010**, *11* (6), 1696–1700.
- (62) Goussé, C.; Chanzy, H.; Excoffier, G.; Soubeyrand, L.; Fleury, E. Stable Suspensions of Partially Silylated Cellulose Whiskers Dispersed in Organic Solvents. *Polymer* **2002**, 43 (9), 2645–2651.
- (63) Kalashnikova, I.; Bizot, H.; Cathala, B.; Capron, I. Modulation of Cellulose Nanocrystals Amphiphilic Properties to Stabilize Oil/Water Interface. *Biomacromolecules* **2012**, *13* (1), 267–275.